Magnetic Field Recovery Technique Based on Distance Weighting Multipole Expansion Method

Li-E Qiang (qianglie@nssc.ac.cn)
National Space Science Center
Binbin Liu
National Space Science Center
Zhen Yang
National Space Science Center
Xiaodong Peng
National Space Science Center
Xiaoshan Ma
National Space Science Center
Peng Xu
Institute of Mechanics
Ziren Luo
Institute of Mechanics
Wenlin Tang
National Space Science Center
Yuzhu Zhang
National Space Science Center
Chen Gao
National Space Science Center

Research Article

Keywords: Magnetic Field Recovery, Space-borne Gravitational Wave Detector, Distance Weighting, Multipole Expansion

Posted Date: April 22nd, 2022

DOI: https://doi.org/10.21203/rs.3.rs-1574780/v1

Magnetic Field Recovery Technique Based on Distance Weighting Multipole Expansion Method

Binbin Liu[1,2], Zhen Yang[1], Li-E Qiang[1*], Xiaodong Peng[1], Xiaoshan Ma[1], Peng Xu[3,4,5], Ziren Luo[3], Wenlin Tang[1], Yuzhu Zhang[1] and Chen Gao[1]

[1*]National Space Science Center, Chinese Academy of Sciences, No.1 Nanertiao Zhongguancun, Beijing, 100190, China.
[2]University of Chinese Academy of Sciences, No.19(A) Yuquan Road, Beijing, 100049, China.
[3]Institute of Mechanics, Chinese Academy of Sciences, No.15 Beisihuanxi Road, Beijing, 100190, China.
[4]Lanzhou Center of Theoretical Physics, Lanzhou University, No.222 South Tianshui Road, Lanzhou, 730000, China.
[5]Hangzhou Institute for Advanced Study, University of Chinese Academy of Sciences, 84 Church Street SE, Hangzhou, 310024, China.

*Corresponding author(s). E-mail(s): qianglie@nssc.ac.cn;
Contributing authors: liubinbin18@mails.ucas.ac.cn; yangzhen@nssc.ac.cn; pxd@nssc.ac.cn; maxs@nssc.ac.cn; xupeng@imech.ac.cn; luoziren@imech.ac.cn; tangwenlin@nssc.ac.cn; zhangyuzhu@nssc.ac.cn; gaochen@nssc.ac.cn;

Abstract

A space-borne gravitational wave detector requires the inertial reference to be in an ultra-low disturbance state, which places exceedingly high demands on the sensitivity of the inertial sensor (IS). However, the local magnetic field of the satellite platform will disturb the test mass (TM) and produce acceleration noise. To monitor and assess the influence of the magnetic field on the TM, it is necessary to monitor the magnetic field near the IS in real-time and reconstruct the magnetic field in the TM area. We propose a distance weighting multipole expansion (DWME) method to satisfy the demand of high-precision magnetic field reconstructions using a small number of magnetometers in a space gravitational wave detection mission. This new method can fully utilize all the magnetometer readout data near two TMs in the spacecraft by distance weighting. The proposed DWME method can reduce the average reconstruction error of a sensitive axial magnetic field from 1.2% to 0.8% and the maximum error from 16% to 8% when compared with the traditional multipole expansion method. Thus, the method provides a new technique to reconstruct the magnetic field using a small number of magnetometers.

Keywords: Magnetic Field Recovery, Space-borne Gravitational Wave Detector, Distance Weighting, Multipole Expansion

1 Introduction

Ground-based gravitational wave detectors first successfully detected gravitational waves (GW) first in 2015[1]; this opened an entirely new window to the universe. Thereafter, scientists devoted themselves to detecting richer sources of GW signals in a wider range of frequencies. As the most interesting sources of GW signals are at low frequencies, space-borne GW detection antennae capable of observing low-frequency signals have received increased attention.

In the early 1990s, the ESA and NASA jointly proposed the Laser Interferometer Space Antenna mission (LISA); this mission comprises an isometric three-spacecraft constellation separated by millions of kilometers to detect the tiny pathlength fluctuations between the spacecraft using intersatellite laser ranging interferometry[2]. Chinese scientists began to make proposals for space-based GW detection in earnest in the 2000s. After years of preliminary study, a complete mission design with 3 million km arms in a heliocentric orbit, the Taiji mission, was officially supported by the Chinese Academy of Sciences in 2016[3–5]. In addition, many other spaceborne GW exploration missions have been proposed, such as ASTROD[6], DECIGO[7], ALIA[8], BBO[9], and Tianqin[10].

An inertial sensor (IS) is one of the core payloads of a space GW detection mission. To detect low frequency GW signals, the test mass (TM) in the IS must maintain free motion along the measurement axis. For LISA and Taiji, the acceleration noise of the TM should be less than $3 \times 10^{-15}\,\mathrm{ms^{-2}\,Hz^{-1/2}}$ in the frequency band of $100\,\mu\mathrm{Hz} - -0.1\,\mathrm{Hz}$[2]. Magnetic field around the TM is one of the main factors contributing to the total acceleration noise allowance of the IS. The stray force on each TM caused by magnetic interference is given by the following formula[11, 12]:

$$\mathbf{F} = \left\langle \left[\left(\mathbf{M} + \frac{\chi}{\mu_0} \mathbf{B} \right) \cdot \boldsymbol{\nabla} \right] \mathbf{B} \right\rangle V, \tag{1}$$

where $\mathbf{M}$ and χ are the remanent magnetic moment and magnetization of the TM, which can be obtained through experimentation[13, 14], μ_0 is the permeability of vacuum, and V is the volume of the TM. $\mathbf{B}$ and $\nabla\mathbf{B}$ are the magnetic field and magnetic field gradient, respectively. The magnetic field $\mathbf{B}$ and the magnetic field gradient $\nabla\mathbf{B}$ at the TM location cannot be calculated by modeling or measured directly with a magnetometer. Furthermore, the magnetic field distribution at the TM location of the GW detection missions in space needs to be reconstructed by interpolation methods, which combine the magnetic field simulation analysis with the readout data of the magnetometer near the TM.

LISA Pathfinder (LPF), which is a precursor mission of LISA, is a technical verification spacecraft for space GW detection missions[15]. It has a magnetic diagnostics subsystem, which includes a set of four fluxgate magnetometers that aim to monitor the magnetic field around the TM location[11, 16]. However, the fluxgate magnetometers used in LPF have a few drawbacks in performing magnetic reconstruction. First, the large size of the sensor and uncertainty in spatial resolution can increase magnetic field reconstruction errors[17], and second, the core of the fluxgate magnetometer contains ferromagnetic material, which generates additional magnetic fields[17, 18]. Therefore, the triaxial fluxgate magnetometers need to be installed away from the TMs and the number of magnetometers needs to be limited. These constraints make it difficult to accurately estimate the magnetic field and gradient in the TMs with the readout data of the fluxgate magnetometers using classical interpolation methods. Choosing high-precision small-sized magnetic sensors with low residual magnetism is one way to resolve the aforementioned problems. Some promising high-sensitivity micromagnetic sensors that can be used in spacecraft for weak magnetic field reconstructions have been investigated[19], such as anisotropic magnetoresistance (AMR)[17, 20–22], tunneling magnetoresistance[23], and giant magnetoresistance [24]. Mateos et al. showed that if the fluxgate magnetometers in the LPF mission were replaced by four AMR sensors $\sim$5cm apart from the TM, the magnetic field reconstruction error would be reduced to less than 15% [25].

Improving the field reconstruction method is another worthwhile approach. The magnetic field reconstruction methods for space GW antennae can be mainly divided into two categories; the first one needs *a priori* information from the magnetic source model, such as the neural network method (see Appendix A.3). Diaz-Aguiló et al. showed that the neural network method can reduce the estimation errors in the magnetic field and gradient to less than 10%[11]. The second is classical interpolation methods such as multipole expansion (ME)[11, 26], distance weighting (DW, see Appendix A.1), and Taylor expansion (TE, see Appendix A.2)[25], which do not rely on *a priori* information about the magnetic structure of the spacecraft. The accuracy of the magnetic field interpolation method is influenced by the number and location of the magnetometers.

In space GW detection, each spacecraft has two TMs separated by tens of centimeters, and each TM is surrounded by several magnetometers. As the reconstruction error of the conventional magnetic field reconstruction method increases with the increase in the magnetometer distance, the magnetometer around the other TM is ignored during the TM magnetic field reconstruction process. In this paper, a distance weighting multipole expansion (DWME) method is proposed to reconstruct the magnetic field at the TM, which suppresses the distance-induced uncertainty by distance weighting and can fully utilize the magnetometer data around the two TMs to achieve more accurate estimates of magnetic field.

The structure of this paper is as follows. Section 2 explains the principle of the DWME method; the simulation results are given in Section 3; and finally, we analyze the results and draw our conclusion in Section 4.

2 The Proposed Multipole Expansion with Distance Weighting

2.1 Magnetic Environment and Sensor Configuration

On a space-borne GW detector spacecraft, the magnetic components are distributed outside the IS area and can be treated as one or more magnetic dipoles. We will use the data on magnetic sources on the LPF given by Astrium[27], which will not affect the performance test of the method. The DC magnetic moment and position of the sources are fixed, but their magnetic moment direction is unknown. Four micromagnetic sensors are placed near each of the two TMs. Figure 1 presents the distribution of the magnetic sources, magnetometers, and TMs. More details are provided in the caption.

According to the theoretical model of magnetic dipoles, the magnetic field generated by the magnetic dipoles at any point $\mathbf{x}$ can be given by

$$\mathbf{B}_r\left(\mathbf{x}\right) = \frac{\mu_0}{4\pi}\sum_{a=1}^{K}\frac{3\left[\mathbf{m}_a\cdot\mathbf{n}_a\right]-\mathbf{m}_a}{\mid \mathbf{x}-\mathbf{x}_{\mathrm{a}}\mid^3}, \tag{2}$$

where K is the quantity of dipoles, $\mathbf{m}_a$ is the moment of the ath magnetic dipole, and $\mathbf{n}_a = \left(\mathbf{x}-\mathbf{x}_{\mathrm{a}}\right)/\mid \mathbf{x}-\mathbf{x}_{\mathrm{a}}\mid$ is a unit vector from dipole $\mathbf{m}_a$ to field point $\mathbf{x}$. The gradient field can therefore be calculated as

$$\frac{\partial B_i}{\partial x_j} = \frac{\mu_0}{4\pi}\sum_{a=1}^{K}\frac{3}{\mid \mathbf{x}-\mathbf{x}_{\mathrm{a}}\mid^4}\left[\left(m_{a,i}n_{a,j}+m_{a,j}n_{a,i}\right)+\left(\mathbf{m}_a\cdot\mathbf{n}_a\right)\left(\delta_{ij}-5n_{a,i}n_{a,j}\right)\right], \tag{3}$$

where δ_{ij} is Kronecker's delta.

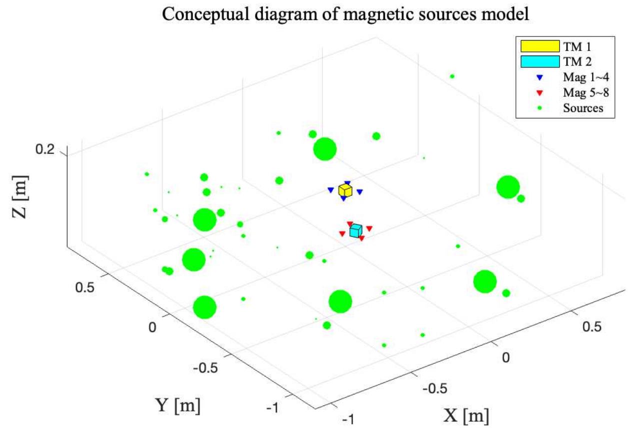

Fig. 1 Spatial distribution of magnetic sources. Magnetic sources: green dots with the size proportional to their moment. TM1: yellow cube with 4 micromagnetic sensors (Mag 1–4 in blue triangle) around it. TM2: cyan cube with 4 micromagnetic sensors (Mag 5–8 in red triangle) around it. The distance between the centers of the TMs is 0.4 m and the included angle is 60°. The side length of TM1 and TM2 is 0.046 m. See Appendix B for more exact location information.

2.2 Distance Weighting Multipole Expansion

As the materials of the components near the TM are almost nonmagnetic, this area can be regarded as a vacuum region. Therefore, its magnetic field has both zero divergence and curl, which means that

$$\mathbf{\nabla} \cdot \mathbf{B}\left(\mathbf{x}\right) = 0,\ \mathbf{\nabla} \times \mathbf{B}\left(\mathbf{x}\right) = 0. \tag{4}$$

We thus get

$$\mathbf{B}\left(\mathbf{x}\right) = \mathbf{\nabla}\Psi\left(\mathbf{x}\right) \tag{5}$$

and

$$\mathbf{\nabla}^2\Psi\left(\mathbf{x}\right) = 0, \tag{6}$$

where $\Psi\left(\mathbf{x}\right)$ is a harmonic scalar function. The solution of this equation can be written as

$$\Psi\left(\mathbf{x}\right) = \sum_{l=0}^{\infty}\sum_{m=-l}^{l} M_{lm} r^l Y_{lm}\left(\mathbf{n}\right), \tag{7}$$

where $r \equiv \mid \mathbf{x} \mid$ and $\mathbf{n} \equiv \mathbf{x}/r$ are the modulus and unit vector of the direction of field point $\mathbf{x}$ in a spherical coordinate system whose origin is set to the center of TM1, respectively. M_{lm} is the multipole coefficient of orders l and m, whereas Y_{lm} is a spherical harmonic function. In Equation (7), terms proportional to

r^{-l-1} can also be included; however, these terms have been omitted as the magnetic field is finite at the geometric center of TM. According to Equations (5) and (7), we have

$$\mathbf{B}(\mathbf{x}) = \boldsymbol{\nabla}\Psi(\mathbf{x}) = \sum_{l=1}^{\infty}\sum_{m=-l}^{l} M_{lm}\boldsymbol{\nabla}\left[r^{l}Y_{lm}(\mathbf{n})\right]. \tag{8}$$

It should be noted that the limited number of magnetometers will lead to a truncation issue in the ME method. Assuming that Equation (8) is truncated at the maximum multipole coefficient order $l = L$, the estimated magnetic field $\mathbf{B}_e$ can be written as

$$\mathbf{B}_e(\mathbf{x}) = \boldsymbol{\nabla}\Psi(\mathbf{x}) = \sum_{l=1}^{L}\sum_{m=-l}^{l} M_{lm}\boldsymbol{\nabla}\left[r^{l}Y_{lm}(\mathbf{n})\right], \tag{9}$$

where the number of multipole coefficients M_{lm} that need to be solved is

$$N_{ME}(L) = \sum_{l=1}^{L}(2l+1) = L(L+2). \tag{10}$$

In addition, each magnetometer can provide magnetic field readings in three channels: (B_x, B_y, B_z). Therefore, the truncation order of ME must satisfy

$$3 \cdot N_{mag} \geq L(L+2), \tag{11}$$

where N_{mag} is the number of magnetometers. For example, multipole coefficients need at least $N_{mag} = 3$ magnetometers to expand to $L = 2$, $N_{mag} = 5$ for $L = 3$, and $N_{mag} = 8$ for $L = 4$.

In the magnetic sources model (MSM) in Figure 1, we can mainly consider the magnetic field reconstruction at the position of TM1. We have 8 magnetometers (Mag 1–8), which theoretically achieve the condition of expansion to $L = 4$, but this will greatly reduce the reconstruction accuracy due to Mag 5–8 being too far away from the TM1 (∼40cm). However, if only Mag 1–4 readouts are used for the magnetic field reconstruction using the traditional ME method, which expands to $L = 2$, the information from Mag 5–8 are omitted. Considering whether the readings of Mag 5–8 are properly processed may help improve the accuracy of the magnetic field reconstruction at TM1. Consequently, we propose a DWME method.

The DWME method selects the optimal multipole coefficient to minimize the error between the reconstruction results and the exact value of the magnetometers. The contribution of the readouts from the nearby magnetometer to the reconstruction error should be greater as they are located near TM1; hence, larger weights are given. Furthermore, small weights are given to the reconstruction error of the distant sensors. The DWME method redefines the error of the traditional ME method in solving multipole coefficients and uses the following distance weighted mean square error:

$$\varepsilon^2 (M_{lm}) = \sum_{s=1}^{N} a_s \mid \mathbf{B}_r (\mathbf{x}_s) - \mathbf{B}_e (\mathbf{x}_s) \mid^2, \tag{12}$$

where a_s is the distance weighting coefficient and $\mathbf{x}_s$ is the position of the magnetometer. An intuitive distance weighting coefficient design is shown in Equation (13).

$$a_s = \frac{1/r_s^n}{\sum_{i=1}^{N} 1/r_i^n}, \tag{13}$$

where n represents the interpolation order and r_i is the distance between the target TM and specified magnetometer. To minimize the error, we let

$$\frac{\partial \varepsilon^2}{\partial M_{lm}} = 0. \tag{14}$$

The optimal estimation of $M_{lm}(t)$ can be calculated using the least square method and we get the estimation of the magnetic field in the whole space by Equation (9). The estimated gradient can be written as

$$\left.\frac{\partial B_i}{\partial x_j}\right|_e (\mathbf{x}) = \sum_{l=0}^{\infty} \sum_{m=-l}^{l} M_{lm} \frac{\partial^2}{\partial x_i \partial x_j} \left[r^l Y_{lm}(\mathbf{n})\right]. \tag{15}$$

2.3 Advanced Distance Weighting Multipole Expansion

As explained in Section 2.2, the DWME method selects and calibrates the optimal weighting order n^* corresponding to the specific MSM in the on-ground experiment. However, when the satellite is on-orbit, there may be an unexpected change in the magnetic moment or even the number of magnetic dipoles, resulting in the n^* of ground calibration no longer being applicable, which will have a negative impact on the magnetic reconstruction. To overcome this weakness of the DWME method in the on-orbit experiment of space GW detection, we propose an advanced distance weighting multipole expansion (ADWME) method.

Briefly, the only difference between ADWME and DWME is the design of the distance weighting coefficient (see Equation (13) for DWME). The distance weighting coefficient $\widetilde{a}_s$ of ADWME can be given as

$$\widetilde{a}_s = \frac{1/r_s^{n(1+\lambda d)}}{\sum_{i=1}^{N} 1/r_i^{n(1+\lambda d)}}, \tag{16}$$

where $d = 1 - \rho$ is the Pearson distance when

$$\rho = \mathrm{Corr}\left(\mathbf{B}_r^{ground}(\mathbf{x}_s), \mathbf{B}_r^{orbit}(\mathbf{x}_s)\right) \in [-1, 1] \tag{17}$$

is the Pearson correlation coefficient between the on-ground calibrated readouts $\mathbf{B}_r^{ground}(\mathbf{x}_s)$ and the on-orbit actual readings $\mathbf{B}_r^{orbit}(\mathbf{x}_s)$ of the magnetometers. Lastly, λ is the sensitivity factor to the changing degree of the MSM.

In other words, the bigger the sensitivity factor, the smaller is the weight of $\widetilde{a}_s$ corresponding to the reading error of the magnetometers near TM2 when $d \neq 0$. Note that λ cannot be too large in order to avoid infinite weight in the calculation process as $r_i < 1$ (see Figure 1). Generally, λ can be set in the range 10—50; in our experiment we let $\lambda = 30$.

3 Results

3.1 Reconstruction of Magnetic Field

To test the performance of the DWME method in an on-ground magnetic field reconstruction task, we randomly selected the direction of a group of magnetic dipoles from two uniform distributions (i.e. $\theta \sim U(0, \pi)$, $\varphi \sim U(0, 2\pi)$) to fix the MSM, and recorded the model as an MSM-Test.

In the process of the magnetic field reconstruction, it is worth noting that the total number of magnetometers satisfied the condition of reconstruction to $L = 4$ (see Equation (11)); however, we truncated the multipole coefficients of the DWME method at $L = 2$ as the magnetometer reading near TM2 is not completely reliable. In addition, according to the DWME method, a small weight was given to the magnetometers' readings near TM2, whereas a large weight was given to the magnetometers' readings near TM1. The selection of the weighting order n in Equation (13) to minimize the error was an intuitive problem. To this end, we studied the influence of the weighting order n on the magnetic field reconstruction error.

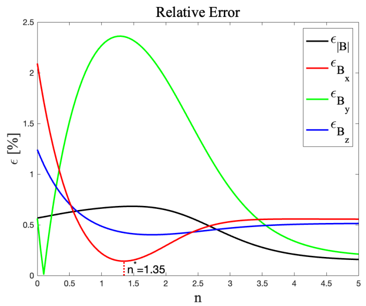

Fig. 2 Relationship between reconstruction error and weighting order n of DWME method. We reconstructed the magnetic field of the MSM-Test model using the DWME method with $L = 2$ for the weighting order n in the range 0–5 with steps of 0.05 and found the optimal weighting order $n^* = 1.35$ corresponding to the minimum error of the MSM-Test model in the direction of the sensitive axis (x-axis).

Figure 2 displays the relationship between the magnetic field reconstruction error and weighting order, defined by[11, 25] as

$$\varepsilon_{|\mathbf{B}|} = \left| \frac{|\mathbf{B}_e| - |\mathbf{B}_r|}{|\mathbf{B}_r|} \right|, \ \varepsilon_{B_j} = \left| \frac{B_{j,e} - B_{j,r}}{|\mathbf{B}_r|} \right|, \tag{18}$$

where $\mid \mathbf{B}_r \mid$ in ε_{B_j} is included to avoid infinite error when the component of the magnetic field is extremely small. As can be seen, all errors (including the error of the magnetic field components and modulus) converged when the weighting order exceeded the third order, whereas the reconstruction error fluctuates for $n \leq 3$. We were especially concerned about the accuracy of the sensitive axis (i.e., the x-axis) as it is the direction of space GW detection. Hence, we chose the optimal weighting order n^*, which minimized the relative percentage error of the magnetic field B_x component. For instance, $n^* = 1.35$ for our MSM-Test.

Next, we simulated the exact magnetic field near TM1 in the $z = 0$ plane, and compared it with the results that employed the DWME method. Figure 3 exhibits the exact magnetic field, estimated field, and error with the DWME method, where the definition of the error is presented in Equation (18). It can be seen that the trends of the left and middle column panels are extremely similar, especially in the TM area (within yellow dotted line), which means that the DWME method can produce a passable precision as well as low relative error (see right column panels in Figure 3).

3.2 Error Analysis

In this section, we summarize the error analysis of different magnetic reconstruction methods in an on-ground magnetic reconstruction environment, which includes the Taylor expansion, distance weighting, multipole expansion, and our DWME method.

Table 1 shows the magnetic reconstruction errors ($\bar{\varepsilon}_{B_j}$ and $\varepsilon_{|B_j|,\max}$, see footnote) between the exact and estimated fields using the aforementioned methods. The first three methods only use magnetometer readings near TM1 (i.e., Mag 1–4) to interpolate the magnetic field, whereas the last five methods use all magnetometer readouts near both TM1 and TM2 (i.e., Mag 1–8). The weighting order n in the DW method, the expansion order k in the TE method, and the expansion order L in the ME method are listed in the chart. In addition, the results were obtained through $N = 10^3$ simulation experiments where the DWME method worked under the condition of adaptive selection of weighting order n^* in steps of 0.05 for each group of magnetic dipoles in direction (θ, φ), which follows the uniform distribution.

As can be seen in Table 1, the DWME method performs best in terms of the reconstruction error in the sensitive axis direction, owing to its selection of the optimal weighting order n^*, which is a highly meaningful option for the space GW detection. Specifically, it reduces the average error by more than 0.4% and the maximum error by over 8% when compared with the other methods. The errors of the first three methods with only four magnetometers are also relatively small in the direction of the sensitive axis. However, the errors of DW, TE, and ME ($L = 2$) methods are improved when all eight magnetometers are used for interpolation. This means that the newly introduced reading information of Mag 5–8 is not conducive to improving the reconstruction accuracy. Moreover, the error of the ME ($L = 4$) with eight magnetometers is larger than

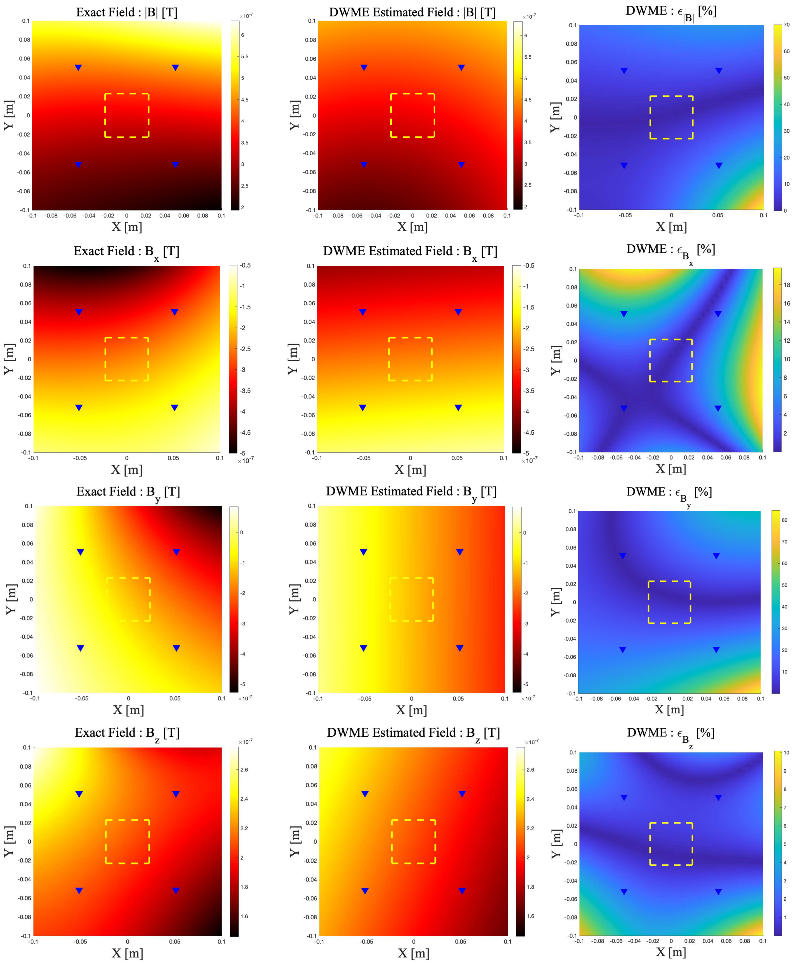

Fig. 3 Contour maps of the accurate (left column), estimated (middle column), and error (right column) of the magnetic field modulus and components obtained by the DWME method with Mag 1–8 in the $z = 0$ plane near TM1 for a specific magnetic sources environment. The outline of TM1 (yellow dotted square with side length of 46 mm) and the location of its nearby magnetometers (Mag 1–4 in blue triangles) are both marked in the plots.

the ME ($L = 2$) with four sensors. This is because the former method uses the magnetometers near TM2, which is far from TM1, to reconstruct the magnetic field until order $L = 4$; this implies the use of the reading information of both Mag 1–4 and Mag 5–8 equally.

However, it is necessary to analyze the reconstruction error of the magnetic component along the sensitive axis with the DWME method under different magnetic source models. As there are few available MSM data, we take the straight line passing through the midpoint of two TMs and parallel to the z-axis as the rotation axis and rotate the magnetic source clockwise once every 30° to obtain 12 sets of MSMs.

Table 1 Relative errors as percentage of the estimated magnetic field at the center of the TM1 using different magnetic reconstruction methods.

Error [%]			$\overline{\varepsilon}_B$ [1]				$\varepsilon_{B,\max}$ [2]			
Method	Order	N_{mag}	$\mid \mathbf{B} \mid$	B_x	B_y	B_z	$\mid \mathbf{B} \mid$	B_x	B_y	B_z
Distance Weighting	n=1		**2.0**	1.2	**1.2**	**1.5**	33	16	44	47
Taylor Expansion	k=1	4	**2.0**	1.2	**1.2**	**1.5**	33	16	44	47
Multipole Expansion	L=2		**2.0**	1.2	**1.2**	**1.5**	33	16	44	47
Distance Weighting	n=1		13	13	15	11	696	799	145	388
Taylor Expansion	k=1		3.0	2.7	2.7	2.3	121	36	83	141
Multipole Expansion	L=2	8	3.0	2.7	2.7	2.3	121	36	83	141
Multipole Expansion	L=4		3.7	5.5	1.7	3.3	39	107	**14**	**35**
Our DWME	L=2		**2.0**	**0.8**	1.7	1.6	**17**	**8**	57	39

Note: The minimum magnetic field reconstruction error in each column of the chart is bold.

[1] $\overline{\varepsilon}_{B_j}$ is the average error calculated as $\overline{\varepsilon}_{B_j} = \frac{1}{N}\sum_{i=1}^{N} \left|B_{j,e}^i - B_{j,r}^i\right| / \mid \mathbf{B}_{j,r} \mid$ relative to $\mid \mathbf{B} \mid$ and B_j, respectively.

[2] The maximum error in percentage for 10^3 randomly selected dipole direction of MSM computed as $\varepsilon_{|B_j|,\max} = \max\limits_{i\in\{1,\ldots,N\}} \left|B_{j,e}^i - B_{j,r}^i\right| / \mid \mathbf{B}_{j,r} \mid$.

Table 2 Comparison of average errors of magnetic field B_x component using several methods under 12 rotation angles of magnetic sources.

Error [%]			$\overline{\varepsilon}_{B_x}$ for different rotation angles											
Method	Order	N_{mag}	$\frac{\pi}{6}$	$\frac{\pi}{3}$	$\frac{\pi}{2}$	$\frac{2\pi}{3}$	$\frac{5\pi}{6}$	π	$\frac{7\pi}{6}$	$\frac{4\pi}{3}$	$\frac{3\pi}{2}$	$\frac{5\pi}{3}$	$\frac{11\pi}{6}$	2π
Distance Weighting	n=1		0.9	1.1	1.6	0.9	2.4	1.3	2.8	1.6	2.2	2.5	1.3	1.2
Taylor Expansion	k=1	4	0.9	1.1	1.6	0.9	2.4	1.3	2.8	1.6	2.2	2.5	1.3	1.2
Multipole Expansion	L=2		0.9	1.1	1.6	0.9	2.4	1.3	2.8	1.6	2.2	2.5	1.3	1.2
Distance Weighting	n=1		14	13	14	11	9.7	7.5	7.6	8.2	8.2	8.1	11	13
Taylor Expansion	k=1		2.8	2.9	3.5	2.0	3.5	2.1	4.3	2.6	3.6	4.0	2.2	2.7
Multipole Expansion	L=2	8	2.8	2.9	3.5	2.0	3.5	2.1	4.3	2.6	3.6	4.0	2.2	2.7
Multipole Expansion	L=4		5.3	5.4	8.2	5.3	4.9	4.3	6.0	3.8	5.3	5.0	4.2	5.5
Our DWME	L=2		**0.4**	**0.6**	**1.1**	**0.4**	**2.1**	**0.9**	**2.5**	**1.2**	**1.9**	**2.3**	**0.7**	**0.8**

Note: Similar to Table 1, the first three methods use only Mag 1–4 readings whereas the other methods use all magnetic sensors. The rotation axis is a straight line parallel to the z-axis through the midpoint of the TMs' centers, i.e., $(-0.1, -0.1732, 0)$. We conducted the experiment by rotating the magnetic sources clockwise around the rotation axis every 30°and obtained 12 groups of MSM after one revolution. The minimum magnetic field reconstruction mean error in each column of the chart is bold.

Table 2 shows the mean errors of the estimated magnetic field component B_x at the TM1 location for the methods mentioned in Table 1 in this experiment. Each error is the average result of 10^3 randomly selected magnetic dipole directions from the uniform distribution. The performance of the DWME method exceeds that of the other methods for the 12 different MSMs, which demonstrates that the DWME method has certain advantages for the estimation of B_x in the on-ground magnetic field reconstruction experiment when compared with other classical methods.

3.3 Robustness Analysis

It should be noted that the advantage of the DWME method in the sensitive axis direction as described in Sections 3.1 and 3.2 comes from the adaptive selection of the optimal weighting order n^*, which depends on the MSM. The weighting order n^* that best fits the magnetic source distribution can be chosen based on ground-based magnetic measurements before launching the spacecraft. However, the characteristics of the magnetic source will change slightly when the satellite is on-orbit. For example, the switching of payload devices may lead to the appearance or disappearance of magnetic units, or some units may change magnetic moment due to a variation in the magnetic environment. To check whether the error of the magnetic field estimates obtained using the DWME method with weighting order n^* remains relatively low during the mission, it is necessary to analyze the robustness of the weighting order.

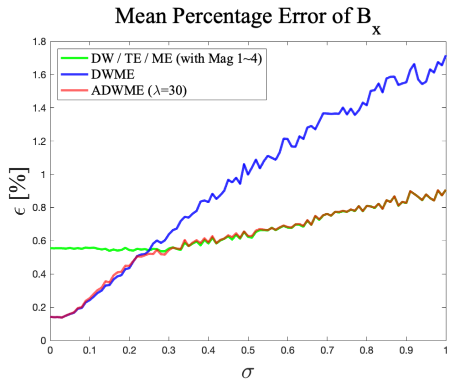

Fig. 4 Quality of the estimate of B_x as a function of the standard devition. σ represents the standard deviation of the truncated normal distribution of the magnetic sources direction parameters (θ, φ) with intervals $[0, \pi]$ and $[0, 2\pi]$, respectively.

Taking the MSM-Test model as an example, the direction of magnetic moment is $\{(\theta_i^*, \varphi_i^*), i = 1, ..., n\}$ and the optimal weighting order of the DWME/ADWME method is $n^* = 1.35$. It is assumed that the variation of the direction parameters $\{(\theta_i, \varphi_i), i = 1, ..., n\}$ of the magnetic dipoles with $\{(\theta_i^*, \varphi_i^*), i = 1, ..., n\}$ as the expectations follow truncated normal distributions with standard deviations $\sigma = \sigma_\theta = \sigma_\varphi$ and intervals $[0, \pi]$ and $[0, 2\pi]$. For each standard deviation σ, 10^3 sets of magnetic parameters $\{(\theta_i, \varphi_i), i = 1, ..., n\}$ are selected to analyze the relationship between the mean estimation errors ε_{B_x} and the standard deviation σ. In Figure 4, the green line corresponds to ε_{B_x}, acquired by classical methods (DW/TE/ME) with 4 magnetometers; the blue line corresponds to ε_{B_x}, acquired by DWME; and the red line corresponds to ε_{B_x}, acquired by ADWME. As can be seen in this figure, when $\sigma < 0.3$, the average relative percentage error of reconstruction by our DWME and ADWME is lower than classical methods (DW/TE/ME) with 4 magnetic sensors. However, the error of DWME method will continue increasing with $0.3 \leq \sigma \leq 1$, whereas the ADWME method with $\lambda = 30$ is almost identical to classical methods. Essentially, the ADWME method combines the merits of both the DWME method and traditional methods. As a result, the ADWME method has good robustness even when there is a large deviation from the initial MSM.

4 Conclusion

In this paper, a new ME method with distance weighting, DWME/ADWME, was proposed. In space GW detection missions, four magnetometers are assumed to be placed around each of the two TMs. The DWME/ADWME method uses all eight magnetometer readings to estimate the magnetic field in the TM area, where the sensors close to the TM are assigned larger weights than those far from the TM. To obtain model-independent results, 10^3 sets of MSMs are selected to perform DWME magnetic field reconstruction experiments. The results show that the average reconstruction error of the magnetic field along the sensitive axis is reduced from 1.2% to 0.8%, and the maximum error is reduced from 16% to 8% compared with the reconstruction error of the conventional ME method. In DWME/ADWME, the optimal weighting order of n^* is dependent on MSM. For any MSM, we can choose an optimal weighting order n_x^* so that the reconstruction error of the B_x component of the magnetic field is minimized. Similarly, the optimal weighting order n_l^* can be chosen so that the reconstruction error of the B_l component of the magnetic field along the l-direction is minimized. In this manner, the DWME/ADWME method can improve the reconstruction accuracy of the magnetic field components in any direction, which allows for a more accurate estimation of the TM magnetic noise in space GW detection missions. It should be emphasized that DWME/ADWME is a general recovery method that can be used not only in magnetic field reconstruction for space GW missions but also in physical fields reconstruction for other missions. The robustness of the weighted order n_x^* in DWME/ADWME is also confirmed. When the MSM does not vary significantly, the DWME reconstruction error of certain magnetic field components at the TM position is smaller than that of the conventional method. However, when the MSM varies greatly, the ADWME method has better robustness.

Appendix A Other Interpolation Methods

A.1 Distance Weighting (DW)

The principle of the DW method is to assign weights to the magnetometers' readings according to the distance from the TM, and then combine them linearly. The expression of the estimated magnetic field at point $\mathbf{x}$ employing the DW method can be given by

$$\mathbf{B}_{\mathrm{e}}\left(\mathbf{x}\right)=\sum_{s=1}^{N}a_s\mathbf{B}_{\mathrm{m}}\left(\mathbf{x}_s\right), \tag{A1}$$

where N is the total number of magnetometers, $\mathbf{B}_{\mathrm{m}}\left(\mathbf{x}_s\right)$ is the readings of the magnetometers, and a_s is the weighting coefficient. See Equation (13) for a common expression of a_s.

A.2 Taylor Expansion (TE)

The TE method is widely used in accurate approximate calculation and can also be adopted to infer the magnetic field at the TM position from the magnetometers' readings. The TE method can be expanded at the center of the TM ($\mathbf{x}_{\mathrm{TM}}$), and the truncation order T of the expansion depends on the number of magnetometers. The magnetic field at the magnetometer position can be expressed as

$$\mathbf{B}_{\mathrm{m}}\left(\mathbf{x}_s\right) = \mathbf{B}_{\mathrm{e}}\left(\mathbf{x}_{\mathrm{TM}}\right) + \sum_{k=1}^{T} \sum_{i=1}^{3} \frac{\partial^k \mathbf{B_e}\left(\mathbf{x}_{\mathrm{TM}}\right)}{\partial x_i^k} \frac{\left(x_{s,i} - x_{\mathrm{TM},\underline{\mathrm{i}}}\right)^k}{k!}, \tag{A2}$$

where $\mathbf{x}_s$ is the positions of the magnetometers and $\mathbf{B}_{\mathrm{m}}\left(\mathbf{x}_s\right)$ is the magnetometers' readouts. $\mathbf{B}_{\mathrm{e}}\left(\mathbf{x}_{\mathrm{TM}}\right)$ and $\frac{\partial^k \mathbf{B}_{\mathrm{e}}(\mathbf{x}_{\mathrm{TM}})}{\partial x_i^k}$ are the magnetic field values and magnetic field gradient at the TM location, respectively, which need to be solved.

According to Equation (4), the magnetic field gradient tensor $\nabla^k B$ is a symmetric traceless matrix that can reduce the number of independent variables. For example, when expanded to the 1st order, the total unknown quantity to be solved is only 8 (3 magnetic field value components and 5 magnetic field gradient value components).

A.3 Artificial Neural Network

The literature [11, 28] indicates that the neural network method takes the reading of the magnetic sensor as the network input, the magnetic field and its gradient at the TM position as the network output; only a fully connected single hidden layer with a small number of neurons can be used to achieve low reconstruction error. The schematic diagram of its network structure is shown in figure A1.

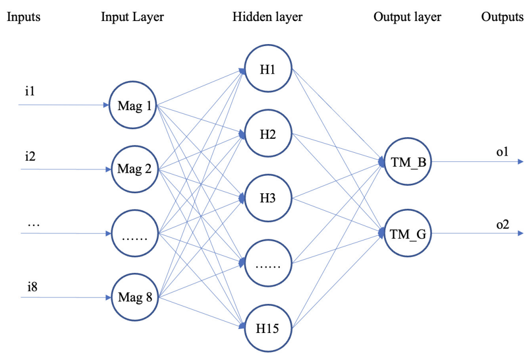

Fig. A1 Basic structure of artificial neural network method

However, the neural network method needs to train with a large number of magnetometers' readings as samples in the ground experiment to obtain high reconstruction accuracy, which is actually an interpolation method with *a priori* information. The moment of each magnetic dipole may change in satellite launching and on-orbit missions, which makes the neural network method face some limitations in generalization ability.

Appendix B Location Information

Table B1 Location of TMs

Name	X(m)	Y(m)	Z(m)
TM1	0	0	0
TM2	-0.2	-0.3464	0

Table B2 Location of magnetometers

Name	X(m)	Y(m)	Z(m)
Mag1	0.0514	0.0514	0
Mag2	0.0514	-0.0514	0
Mag3	-0.0514	0.0514	0
Mag4	-0.0514	-0.0514	0
Mag5	-0.1298	-0.3652	0
Mag6	-0.2188	-0.4166	0
Mag7	-0.1812	-0.2762	0
Mag8	-0.2702	-0.3276	0

Declarations

- **Funding** This work is supported by the National Key Research and Development Program of China No.2020YFC2200603, No.2020YFC2201303, No.2020YFC2200102, No.2020YFC2200601 and No.2020YFC2200104, the Youth Fund Project of National Natural Science Foundation of China No. 11905017, the Strategic Priority Research Program of the Chinese Academy of Sciences Grant No.XDA1502110102-04 and No.XDA1502110101-01.
- **Conflict of interest/Competing interests** The authors have no conflicts of interest to declare that are relevant to the content of this article.
- **Availability of data and materials** Authors agree to make data and materials supporting the results or analyses presented in their paper available upon reasonable request.
- **Authors' contributions** All authors contributed to the study conception and design. Theoretical analysis and simulation experiment were performed by Binbin Liu. The first draft of the manuscript was written by Binbin Liu, Zhen Yang, Li-E Qiang, Xiaodong Peng and Xiaoshan Ma. Li-E Qiang, Peng Xu and Ziren Luo provided theoretical guidance. Wenlin Tang, Yuzhu Zhang and Chen Gao checked and provided guidance on the analysis of the experimental results. All authors reviewed the manuscript.
- **Ethics approval** Not applicable.
- **Consent to participate** Not applicable.
- **Consent for publication** Not applicable.

References

[1] Abbott BP, Abbott R, Abbott T, Abernathy M, Acernese F, Ackley K, et al. Observation of gravitational waves from a binary black hole merger. Physical review letters. 2016;116(6):061102.

[2] Amaro-Seoane P, Audley H, Babak S, Baker J, Barausse E, Bender P, et al. Laser interferometer space antenna. arXiv preprint arXiv:170200786. 2017;.

[3] Xue-Fei G, Sheng-Nian X, Ye-Fei Y, Shan B, Xing B, Zhou-Jian C, et al. Laser interferometric gravitational wave detection in space and structure formation in the early universe. Chinese Astronomy and Astrophysics. 2015;39(4):411–446.

[4] Hu WR, Wu YL. Taiji Program in Space for Gravitational Wave Physics and Nature of Gravity. National Science Review. 2017;.

[5] Luo Z, Guo Z, Jin G, Wu Y, Hu W. A brief analysis to Taiji: Science and technology. Results in Physics. 2020;16:102918.

[6] Ni WT. ASTROD-GW: Overview and progress. International Journal of Modern Physics D. 2013;22(01):1341004.

[7] Seto N, Kawamura S, Nakamura T. Possibility of direct measurement of the acceleration of the universe using 0.1 Hz band laser interferometer gravitational wave antenna in space. Physical Review Letters. 2001;87(22):221103.

[8] Bender PL. Additional astrophysical objectives for LISA follow-on missions. Classical and Quantum Gravity. 2004;21(5):S1203.

[9] Phinney S, Bender P, Buchman R, Byer R, Cornish N, Fritschel P, et al. The Big Bang Observer: Direct detection of gravitational waves from the birth of the Universe to the Present. NASA Mission Concept Study. 2004;.

[10] Luo J, Chen LS, Duan HZ, Gong YG, Hu S, Ji J, et al. TianQin: a space-borne gravitational wave detector. Classical and Quantum Gravity. 2016;33(3):035010.

[11] Diaz-Aguiló M, García-Berro E, Lobo A. Theory and modelling of the magnetic field measurement in LISA PathFinder. Classical and quantum gravity. 2010;27(3):035005.

[12] Diaz-Aguiló M, Mateos I, Ramos-Castro J, Lobo A, García-Berro E. Design of the magnetic diagnostics unit onboard LISA Pathfinder. Aerospace science and technology. 2013;26(1):53–59.

[13] Hueller M, Armano M, Carbone L, Cavalleri A, Dolesi R, Hoyle C, et al. Measuring the LISA test mass magnetic properties with a torsion pendulum. Classical and Quantum Gravity. 2005;22(10):S521.

[14] Diaz-Aguiló M, García-Berro E, Lobo A. Inflight magnetic characterization of the test masses onboard LISA Pathfinder. Physical Review D. 2012;85(4):042004.

[15] Antonucci F, Armano M, Audley H, Auger G, Benedetti M, Binetruy P, et al. LISA Pathfinder: mission and status. Classical and Quantum Gravity. 2011;28(9):094001.

[16] Canizares P, Conchillo A, García-Berro E, Gesa L, Grimani C, Lloro I, et al. The diagnostics subsystem on board LISA Pathfinder and LISA. Classical and Quantum Gravity. 2009;26(9):094005.

[17] Mateos I, Diaz-Aguiló M, Gesa L, Gibert F, Karnesis N, Lloro I, et al. Magnetic field measurement using chip-scale magnetometers in eLISA. In: Journal of Physics: Conference Series. vol. 610. IOP Publishing; 2015. p. 012028.

[18] Mateos I, Diaz-Aguiló M, Gibert F, Lloro I, Lobo A, Nofrarias M, et al. Magnetic back action effect of magnetic sensors for eLISA/NGO. nTm. 2013;3(1 S 1):2.

[19] Ripka P, Janosek M. Advances in magnetic field sensors. IEEE Sensors journal. 2010;10(6):1108–1116.

[20] Hauser H, Fulmek PL, Haumer P, Vopalensky M, Ripka P. Flipping field and stability in anisotropic magnetoresistive sensors. Sensors and Actuators A: Physical. 2003;106(1-3):121–125.

[21] Mateos I, Diaz-Aguiló M, Gibert F, Lloro I, Lobo A, Nofrarias M, et al. Temperature coefficient improvement for low noise magnetic measurements in LISA. In: Journal of Physics: Conference Series. vol. 363. IOP Publishing; 2012. p. 012051.

[22] Martın IM. Design and assessment of a low-frequency magnetic measurement system for eLISA. 2015;.

[23] Luong VS, Chang CH, Jeng JT, Lu CC, Hsu JH, Chang CR. Reduction of low-frequency noise in tunneling-magnetoresistance sensors with a modulated magnetic shielding. IEEE Transactions on Magnetics. 2014;50(11):1–4.

[24] Dufay B, Saez S, Dolabdjian C, Yelon A, Ménard D. Development of a high sensitivity giant magneto-impedance magnetometer: Comparison with a commercial flux-gate. IEEE Transactions on magnetics. 2012;49(1):85–88.

[25] Mateos I, Díaz-Aguiló M, Ramos-Castro J, García-Berro E, Lobo A. Interpolation of the magnetic field at the test masses in eLISA. Classical and Quantum Gravity. 2015;32(16):165003.

[26] Díaz Aguiló M, García-Berro Montilla E, Lobo Gutiérrez JA. LTP Magnetic Field Interpolation. 2010;.

[27] Díaz Aguiló M. Magnetic diagnostics algorithms for LISA pathfinder: system identification and data analysis. 2011;.

[28] Diaz-Aguilo M, Lobo A, García-Berro E. Neural network interpolation of the magnetic field for the LISA Pathfinder Diagnostics Subsystem. Experimental Astronomy. 2011;30(1):1–21.